Journal of Thermal Stresses
Publication details, including instructions for authors and subscription information:
http://www.informaworld.com/smpp/title~content=t713723680

Laser-Generated Thermoelastic Waves in an Anisotropic Infinite Plate: FEM Analysis

Hussain M. Al-Qahtani [a]; Subhendu K. Datta [a]; Osama M. Mukdadi [b]
[a] Department of Mechanical Engineering, University of Colorado, Boulder. Boulder, Colorado. USA
[b] Department of Pediatric Cardiology, The Children's Hospital. Denver, Colorado. USA

To cite this Article: Al-Qahtani, Hussain M., Datta, Subhendu K. and Mukdadi, Osama M. , 'Laser-Generated Thermoelastic Waves in an Anisotropic Infinite Plate: FEM Analysis', Journal of Thermal Stresses, 28:11, 1099 - 1122
To link to this article: DOI: 10.1080/014957390967848
URL: http://dx.doi.org/10.1080/014957390967848

Journal of Thermal Stresses, 28: 1099–1122, 2005

ISSN: 0149-5739 print/1521-074X online
DOI: 10.1080/014957390967848

Taylor & Francis
Taylor & Francis Group

LASER-GENERATED THERMOELASTIC WAVES IN AN ANISOTROPIC INFINITE PLATE: FEM ANALYSIS

Hussain M. Al-Qahtani and Subhendu K. Datta
Department of Mechanical Engineering, University of Colorado, Boulder, Colorado, USA

Osama M. Mukdadi
Department of Pediatric Cardiology, The Children's Hospital, Denver, Colorado, USA

In recent years, the study of thermoelastic waves generated by focused laser beams has been undertaken by several researchers because the technique provides a means for noncontact generation of ultrasonic waves. Laser-generated ultrasonic waves have diverse applications ranging from material characterization to nondestructive testing of defects. Transient ultrasonic guided waves generated in an anisotropic infinite plate by a pulsed laser beam are investigated in this study. A semi-analytical finite element method (SAFEM) is adopted for this purpose. In this method, the plate is divided into parallel layers through its thickness and the displacement and temperature in each layer are approximated by quadratic polynomials in the thickness direction (z). They are assumed to be continuous functions of time and in-plane cartesian coordinates (x, y). Transient response is calculated using Fourier transformations in time and space variables (x, y). The analysis technique is applicable to a generally anisotropic plate. Results for dispersion of guided waves and transient displacement in infinite silicon nitride (Si_3N_4) plates are presented. Numerical results show that for the assumed form of heat deposition by the laser mainly the lowest Lamb modes, namely, the lowest symmetric (S_0) and antisymmetric (A_0) modes, are excited. They also show that the transient response is dominated by the antisymmetric mode A_0, which shows characteristic dispersion. This study provides a quantitative model for laser-generated thermoelastic waves in an anisotropic plate and can be used for nondestructive evaluation.

Keywords: Laser; Thermoelastic; Lamb wave; Anisotropy; Plate

INTRODUCTION

Since ultrasonic guided elastic waves propagate long distances in structures, they provide an efficient means of characterization of anisotropic properties of engineering structures, such as elastic and thermal properties. Guided waves can also be used for material characterization of layered and composite structures. The other important application of ultrasonic waves is in defect detection. Presence and size of various defects and discontinuities such as cracks, inclusions, and porosity can be

Received 3 December 2004; accepted 14 January 2005.
Address correspondence to Subhendu K. Datta, Department of Mechanical Engineering, University of Colorado, Boulder, CO 80309-0427, USA. E-mail: dattas@spot.colorado.edu

precisely measured. Furthermore, ultrasonic waves can be used to measure dimensional properties. For instance, plate thickness can be accurately measured by the "time-of-flight" of ultrasonic waves.

A laser beam focused on a small region of the surface of a plate (or other structure) generates thermal and elastic waves in the plate. Such waves generated by a pulsed laser operating in the thermoelastic regime are highly suitable for noncontact nondestructive evaluation. The laser source can be operated away from hot, corrosive, or other hazardous environment [1].

In 1963, White [2] demonstrated that ultrasonic waves can be generated by irradiating a surface by laser beam. Since then, significant work has been done on the modeling and experiment of laser ultrasonics. It was shown by Sontag and Tam [3] that Lamb waves can be generated and detected by laser techniques. They studied Lamb waves in silicon wafers. Their work was extended by Hutchins et al. [4] for the determination of the thickness of metal sheets. Dewhurst et al. [5] used a pulsed laser to generate both symmetric and antisymmetric Lamb waves. These waves were optically detected with a laser interferometer, and the sheet thickness was determined with great accuracy.

In contrast with the abundant theoretical and experimental studies of laser-generated bulk waves, studies of Lamb waves in plates are mostly experimental. Among the limited theoretical studies is that of Spicer et al. [6], who investigated Lamb waves in a thin isotropic plate using Laplace-Hankel transforms. Normal mode technique was used by Weaver and Pao [7] to study the isothermal displacement generated by a point load applied to a plate. More recently, the same method, also known as the method of eigenfunction expansion, has been used by several researchers [8–10].

The objective of this work is to present an analysis of dynamic thermoelastic wave propagation in an anisotropic plate. An earlier study by Arias and Achenbach [11] on transient response of an isotropic half-space suggests that such an analysis should consider the coupled thermoelastic problem including the spatial distribution of the heat generated by a pulsed laser. This article treats this thermoelastic problem for a plate. In this, a thermal relaxation time is included in the heat conduction equation so that the thermal wave speed is finite. As in Arias and Achenbach [11], a line-focused laser source is considered.

A semi-analytical finite element method (SAFEM) is adopted to model the guided waves generated in infinite anisotropic plates. The plate is divided into several parallel sublayers, within each of which the temperature and displacement are approximated by quadratic polynomials in the thickness coordinate (z), and they are assumed to be continuous functions of time and the planar coordinates (x, y). Then, the system of homogeneous equation of motion and heat conduction leads to an algebraic eigenvalue problem for the determination of the wave numbers of guided waves at a fixed frequency. This has been reported in an earlier work [12]. Once the wave number-frequency equation (the dispersion equation) is solved, the transient response is obtained by using Fourier transform. The transient response thus obtained is in the wave number-frequency domain. The response in the space-time domain is then obtained by numerically evaluating the double inverse Fourier transforms. Cauchy's residue theorem is used to first express the wave number integral as a sum of the modal contributions at a given frequency. Then, a fast Fourier transform leads to the time response.

The article is organized in the following manner. Theoretical formulations are presented first, followed by numerical results and discussion. The article concludes with some remarks and suggestions for future work.

MATHEMATICAL FORMULATION

We consider an infinite homogeneous transversely isotropic thermally conducting elastic plate at a uniform temperature T_0 in the undisturbed state having a thickness H (see Figure 1). The displacement and temperature are assumed to be functions of x, y, z, and t. The displacement in the x, y, and z directions are denoted by u, v, and w, respectively.

The heat conduction equation is assumed to be governed by the Lord-Shulman (L-S) theory of thermoelasticity containing a single relaxation time [13]. The governing equations may be summarized as follows:

(1) Equations for momentum and heat conduction, respectively, are

$$\sigma_{ij,j} + f_i = \rho \ddot{u}_i \quad \text{in } \Omega \tag{1}$$

$$\rho T_0 \dot{\eta} + Q = -q_{k,k} \quad \text{in } \Omega \tag{2}$$

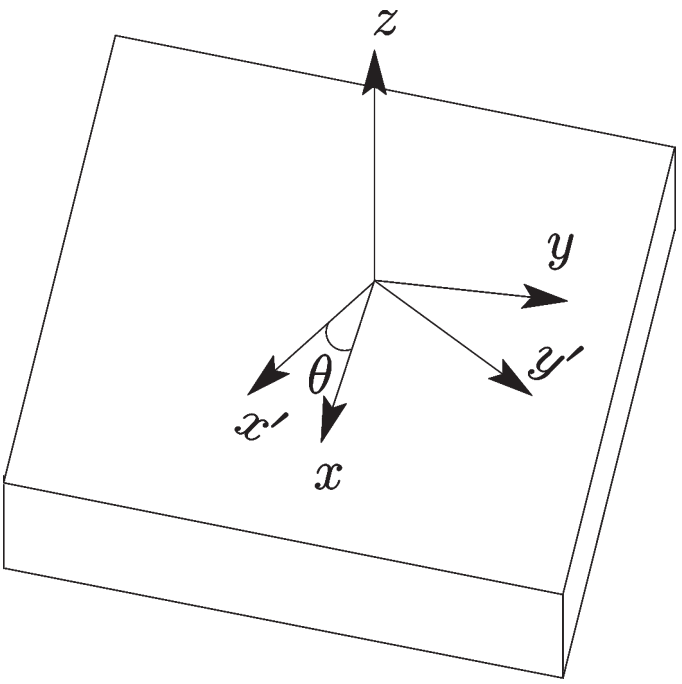

Figure 1 Geometry of the problem.

(2) Constitutive and kinematic equations:

$$\sigma_{ij} = c_{ijkl}\epsilon_{kl} - \beta_{ij}T \tag{3}$$

$$q_i + \tau_0 \dot{q}_i = -K_{ij}T_{,j} \tag{4}$$

$$\rho\dot{\eta} = \beta\dot{\epsilon} + \frac{\rho C_E}{T_0}\dot{T} \tag{5}$$

$$\epsilon_{ij} = \frac{1}{2}(u_{i,j} + u_{j,i}) \tag{6}$$

Note that Fourier law of heat conduction has been modified to account for the finite speed of the thermal wave by introducing the relaxation time τ_0.

(3) Initial and boundary conditions:

$$\sigma_{ij}n_j = 0 \quad \text{in } \Gamma_\sigma \tag{7}$$

$$q_i n_i = 0 \quad \text{in } \Gamma_q \tag{8}$$

$$u_i = 0 \quad \text{at } t = 0 \tag{9}$$

$$\dot{u}_i = 0 \quad \text{at } t = 0 \tag{10}$$

The physical variables and material constants appearing in the above equations are:

σ_{ij}	stress tensor	ϵ_{ij}	components of strain tensor
K_{ij}	coefficients of thermal conductivity	c_{ijkl}	elastic constants
β_{ij}	thermal coefficients	T	temperature perturbation
q_i	heat flux	ρ	mass density
τ_0	thermal relaxation time	η	entropy density
C_E	specific heat at constant deformation	T_0	reference temperature
Q	heat source	f	mechanical body force
Ω	domain	$\Gamma_{\sigma,q}$	stress and thermal boundaries
n_j	outward unit normal	t	time

A comma $(,i)$ and the superposed dot $(\cdot)$ represents a partial derivative with respect to the cartesian coordinate x_i and the time, respectively.

The plate is divided into N parallel, homogeneous, and perfectly bonded anisotropic layers. A global rectangular coordinate system (X, Y, Z) is used such that X and Y axes lie in the mid-plane of the plate, and the Z axis is parallel to the thickness direction of the plate (see Figure 2). In each layer, a system of local coordinate axes (x, y, z) that are parallel to the global (X, Y, Z) axes is chosen.

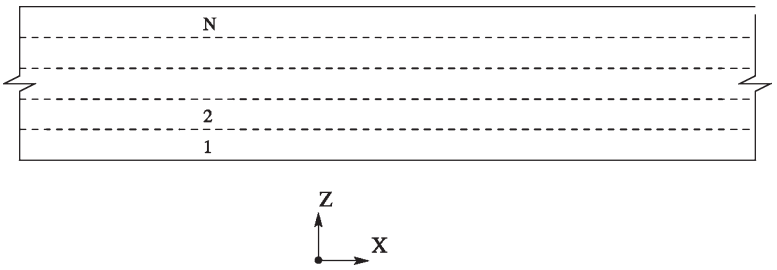

Figure 2 Discretization of the plate across the thickness.

Two sets of shape functions are introduced to approximate the displacement and temperature in each layer, namely,

$$\mathbf{u}(x,y,z,t) = N_1^e(z)\mathbf{u}^e(x,y,t) \tag{11}$$

$$\mathbf{T}(x,y,z,t) = N_2^e(z)\mathbf{T}^e(x,y,t) \tag{12}$$

where

$$N_1^e = \begin{bmatrix} N_1 & 0 & 0 & N_2 & 0 & 0 & N_3 & 0 & 0 \\ 0 & N_1 & 0 & 0 & N_2 & 0 & 0 & N_3 & 0 \\ 0 & 0 & N_1 & 0 & 0 & N_2 & 0 & 0 & N_3 \end{bmatrix} \tag{13}$$

and

$$N_2^{e^T} = \{N_1 \; N_2 \; N_3\} \tag{14}$$

Nodal displacements and temperatures are stored in the two vectors $\mathbf{u}^e$ and T^e, respectively. Using generalized linear thermoelasticity, the strain tensor and temperature vector are derived from the kinematic equations

$$\epsilon = \mathbf{D}_1\mathbf{u}^e_{,x} + \mathbf{D}_2\mathbf{u}^e_{,y} + \mathbf{D}_3\mathbf{u}^e \tag{15}$$

$$\mathbf{T}' = \mathbf{B}_1\mathbf{T}^e_{,x} + \mathbf{B}_2\mathbf{T}^e_{,y} + \mathbf{B}_3\mathbf{T}^e \tag{16}$$

where $\mathbf{B}_1$, $\mathbf{B}_2$, $\mathbf{B}_3$, $\mathbf{D}_1$, $\mathbf{D}_2$, and $\mathbf{D}_3$ are defined in the appendix and $\mathbf{T}'$ is the temperature gradient.

Taking the variation of Eqs. (15)–(16), we obtain

$$\delta\epsilon = \mathbf{D}_1\delta\mathbf{u}^e_x + \mathbf{D}_2\delta\mathbf{u}^e_y + \mathbf{D}_3\delta\mathbf{u}^e \tag{17}$$

$$\delta\mathbf{T}' = \mathbf{B}_1\delta\mathbf{T}^e_{,x} + \mathbf{B}_2\delta\mathbf{T}^e_{,y} + \mathbf{B}_3\delta\mathbf{T}^e \tag{18}$$

The variational principle for the thermoelastic problem can be written (using vector notation) in the following form:

$$\int_{t_0}^{t_1}\int_V (\delta\epsilon^T\sigma - \delta\mathbf{T}'^T\mathbf{K}\mathbf{T}' - \delta\mathbf{T}'^T(\mathbf{q} + \tau_0\dot{\mathbf{q}}))\mathrm{d}V\,\mathrm{d}t = \int_{t_0}^{t_1}\int_V \delta\mathbf{u}^T(\mathbf{f} - \rho\ddot{\mathbf{u}})\mathrm{d}V\,\mathrm{d}t \tag{19}$$

Substituting the constitutive relations (Eqs. (3–6)) into Eq. (19), the following equations are obtained:

$$\begin{aligned}
\int_{t_0}^{t_1}\int_V \delta\epsilon^T\sigma \mathbf{d}V\,\mathbf{d}t &= \int_{t_0}^{t_1}\int_V \delta\epsilon^T(\mathbf{C}\epsilon-\beta\mathbf{T})\mathrm{d}V\,\mathrm{d}t\\
&= \int_{t_0}^{t_1}\int_V [(\delta\mathbf{u}_{,x}^{eT}\mathbf{D}_1^T+\delta\mathbf{u}_{,y}^{eT}\mathbf{D}_2^T+\delta\mathbf{u}^{eT}\mathbf{D}_3^T)\mathbf{C}(\mathbf{D}_1\delta\mathbf{u}_{,x}^{e}+\mathbf{D}_2\delta\mathbf{u}_{,y}^{e}+\mathbf{D}_3^T\delta\mathbf{u}^{e})\\
&\quad -(\mathbf{u}_{,x}^{eT}\mathbf{D}_1^T+\mathbf{u}_{,x}^{eT}\mathbf{D}_2^T+\mathbf{u}^{eT}\mathbf{D}_3^T)\beta\mathrm{N}_2^{eT}\mathbf{T}^e]\mathrm{d}V\,\mathrm{d}t\\
&= \int_{t_0}^{t_1}\int_y\int_x \delta\mathbf{u}^{eT}\Big[-\mathbf{k}_{11}^e\mathbf{u}_{,xx}^e-\mathbf{k}_{12}^e\mathbf{u}_{,xy}^e-\mathbf{k}_{13}^e\mathbf{u}_{,x}^e-\mathbf{k}_{21}^e\mathbf{u}_{,xy}^e-\mathbf{k}_{22}^e\mathbf{u}_{,yy}^e-\mathbf{k}_{23}^e\mathbf{u}_{,y}^e+\mathbf{k}_{31}^e\mathbf{u}_{,x}^e\\
&\qquad +\mathbf{k}_{32}^e\mathbf{u}_{,y}^e+\mathbf{k}_{33}^e\mathbf{u}_{,yy}^e+\mathbf{k}_{m01}^e\mathbf{T}_{,x}^e+\mathbf{k}_{m02}^e\mathbf{T}_{,y}^e-\mathbf{k}_{m03}^e\mathbf{T}_{,x}^e\Big]\mathrm{d}x\,\mathrm{d}y\,\mathrm{d}t \qquad (20)
\end{aligned}$$

where the element matrices appearing in the last equation are defined in the appendix. The second term on the left-hand side of Eq. (19) can be written as

$$\begin{aligned}
\int_{t_0}^{t_1}\int_V \delta(\mathbf{T}^{eT})'\mathbf{K}(\mathbf{T}^e)'\mathrm{d}V\,\mathrm{d}t &= \int_{t_0}^{t_1}\int_V(\delta\mathbf{T}_{,x}^{eT}\mathbf{B}_1^T+\delta\mathbf{T}_{,y}^{eT}\mathbf{B}_2^T+\delta\mathbf{T}^{eT}\mathbf{B}_3^T)\mathbf{K}\\
&\qquad\times(\mathbf{B}_1\mathbf{T}_{,x}^e+\mathbf{B}_2\mathbf{T}_{,y}^e+\mathbf{B}_3\mathbf{T}^e)\mathrm{d}V\mathrm{d}t\\
&= \int_{t_0}^{t_1}\int_y\int_x \delta\mathbf{T}^{eT}(\mathbf{g}_{11}^e\mathbf{T}_{,xx}^e+\mathbf{g}_{22}^e\mathbf{T}_{,yy}^e-\mathbf{g}_{33}^e\mathbf{T}^e)\mathrm{d}x\,\mathrm{d}y\,\mathrm{d}t \qquad (21)
\end{aligned}$$

where $\mathbf{g}_{11}$, $\mathbf{g}_{22}$, and $\mathbf{g}_{33}$ are defined by

$$\mathbf{g}_{11}^e=\int_z \mathbf{B}_1^T\mathbf{K}\mathbf{B}_1\mathrm{d}z,\qquad \mathbf{g}_{22}^e=\int_z \mathbf{B}_2^T\mathbf{K}\mathbf{B}_2\mathrm{d}z,\qquad \mathbf{g}_{33}^e=\int_z \mathbf{B}_3^T\mathbf{K}\mathbf{B}_3\mathrm{d}z$$

The third term on the left-hand side of Eq. (19) is

$$\begin{aligned}
&\int_{t_0}^{t_1}\int_V \delta(\mathbf{T}^{eT})'(\mathbf{q}+\tau_0\dot{\mathbf{q}})\mathrm{d}V\,\mathrm{d}t\\
&\quad= -\int_{t_0}^{t_1}\int_V \delta\mathbf{T}^{eT}(\mathbf{q}'+\tau_0\dot{\mathbf{q}}')\mathrm{d}V\,\mathrm{d}t\\
&\quad= \int_{t_0}^{t_1}\int_V \delta\mathbf{T}^{eT}(\mathrm{T}_0\rho\dot{\boldsymbol{\eta}}+\tau_0\mathrm{T}_0\rho\ddot{\boldsymbol{\eta}}+Q+\tau_0\dot{Q})\mathrm{d}V\,\mathrm{d}t\\
&\quad= \int_{t_0}^{t_1}\int_y\int_x \delta\mathbf{T}^{eT}[(\mathbf{f}_1^e\dot{\mathbf{u}}_{,x}^e+\mathbf{f}_2^e\dot{\mathbf{u}}_{,y}^e+\mathbf{f}_3^e\dot{\mathbf{u}}^e+\mathbf{m}_{\theta\theta}^e\dot{\mathbf{T}})\\
&\qquad\qquad +\tau_0(\mathbf{f}_1\ddot{\mathbf{u}}_{,x}^e+\mathbf{f}_2\ddot{\mathbf{u}}_{,y}^e+\mathbf{f}_3\ddot{\mathbf{u}}^e+\mathbf{m}_{\theta\theta}^e\ddot{\mathbf{T}}+Q_{th})]\mathrm{d}x\,\mathrm{d}y\,\mathrm{d}t \qquad (22)
\end{aligned}$$

where $\mathbf{q}'=q_{i,i,}$ Q_{th} is the thermal load, and

$$\mathbf{m}_{\theta\theta}^e=\int_z N_2^e\rho N_2^{eT}\mathrm{d}z,\qquad \mathbf{f}_1^e=\int_z T_0N_2^e\beta\mathbf{D}_1\mathrm{d}z,$$

$$\mathbf{f}_2^e = \int_z T_0 N_2^e \beta \mathbf{D}_2 \mathrm{d}z, \qquad \mathbf{f}_3^e = \int_z T_0 N_2^e \beta \mathbf{D}_3 \mathrm{d}z$$

The right-hand side of Eq. (19) is written as

$$\begin{aligned}\int_{t_0}^{t_1}\int_V \delta\mathbf{u}^T(\mathbf{f} - \rho\ddot{\mathbf{u}})\mathrm{d}V\ \mathrm{d}t &= \int_{t_0}^{t_1}\int_V \delta\mathbf{u}^{eT} N_1^{eT}(\mathbf{f} - \rho N_1^e \ddot{\mathbf{u}}^e)\mathrm{d}V\ \mathrm{d}t \\ &= \int_{t_0}^{t_1}\int_y\int_x \delta\mathbf{u}^{eT}(\mathbf{f}^e - \mathbf{m}^e\ddot{\mathbf{u}}^e)\mathrm{d}x\ \mathrm{d}y\ \mathrm{d}t \end{aligned} \tag{23}$$

where

$$\mathbf{f}^e = \int_z N_1^{eT}\mathbf{f}\mathrm{d}z, \qquad \mathbf{m} = \int_z \rho N_1^{eT} N_1^e \mathrm{d}z$$

Equating the coefficient of $\delta\mathbf{u}^e$ in Eq. (19) to zero yields

$$\begin{aligned}&\mathbf{k}_{11}^e\mathbf{u}_{,xx}^e + \mathbf{k}_{12}^e\mathbf{u}_{,xy}^e + \mathbf{k}_{13}^e\mathbf{u}_{,x}^e + \mathbf{k}_{21}^e\mathbf{u}_{,xy}^e + \mathbf{k}_{22}^e\mathbf{u}_{,yy}^e + \mathbf{k}_{23}^e\mathbf{u}_{,y}^e - \mathbf{k}_{31}^e\mathbf{u}_{,x}^e \\ &\quad - \mathbf{k}_{32}^e\mathbf{u}_{,y}^e - \mathbf{k}_{33}^e\mathbf{u}^e - \mathbf{k}_{m01}^e\mathbf{T}_{,x}^e - \mathbf{k}_{m02}^e\mathbf{T}_{,y}^e + \mathbf{k}_{m03}^e\mathbf{T}^e - \mathbf{m}^e\ddot{\mathbf{u}}^e = \mathbf{f}^e \end{aligned} \tag{24}$$

Similarly, equating the coefficient of $\delta\mathbf{T}^e$ in Eq. (19) yields

$$\begin{aligned}&\tau_0\mathbf{m}_{\theta\theta}^e\ddot{\mathbf{T}}^e + \mathbf{m}_{\theta\theta}^e\dot{\mathbf{T}}^e + \tau_0\mathbf{f}_1^e\ddot{\mathbf{u}}_{,x}^e + \tau_0\mathbf{f}_2^e\ddot{\mathbf{u}}_{,y}^e + \tau_0\mathbf{f}_3^e\ddot{\mathbf{u}}^e + \mathbf{f}_1^e\dot{\mathbf{u}}_{,x}^e + \mathbf{f}_2^e\dot{\mathbf{u}}_{,y}^e \\ &\quad + \mathbf{f}_3^e\dot{\mathbf{u}}^e - \mathbf{g}_{11}^e\mathbf{T}_{,xx}^e - \mathbf{g}_{22}^e\mathbf{T}_{,yy}^e + \mathbf{g}_{33}^e\mathbf{T}^e = \mathbf{Q}^e \end{aligned} \tag{25}$$

The last two equations (Eq. (24) and Eq. (25)) are written in vector form as

$$\begin{aligned}&[-\mathbf{M}\ 0]\begin{Bmatrix}\ddot{\mathbf{u}}^e \\ \ddot{\mathbf{T}}^e\end{Bmatrix} + [\mathbf{K}_{11}\ 0]\begin{Bmatrix}\mathbf{u}_{,xx}^e \\ \mathbf{T}_{,xx}^e\end{Bmatrix} + [\mathbf{K}_{12} + \mathbf{K}_{21}\ 0]\begin{Bmatrix}\mathbf{u}_{,xy}^e \\ \mathbf{T}_{,xy}^e\end{Bmatrix} \\ &\quad + [\mathbf{K}_{13} - \mathbf{K}_{31}\ -\mathbf{K}_{m01}]\begin{Bmatrix}\mathbf{u}_{,x}^e \\ \mathbf{T}_{,x}^e\end{Bmatrix} + [\mathbf{K}_{22}\ 0]\begin{Bmatrix}\mathbf{u}_{,yy}^e \\ \mathbf{T}_{,yy}^e\end{Bmatrix} \\ &\quad + [\mathbf{K}_{23} - \mathbf{K}_{32}\ -\mathbf{K}_{m02}]\{\mathbf{u}_{,y}^e\mathbf{T}_{,y}^e\} + [-\mathbf{K}_{33}\ \mathbf{K}_{m03}]\begin{Bmatrix}\mathbf{u}^e \\ \mathbf{T}^e\end{Bmatrix} = \mathbf{f}^e \end{aligned} \tag{26}$$

and

$$\begin{aligned}&[\tau_0\mathbf{F}_3\ \tau_0\mathbf{F}_{\theta\theta}]\begin{Bmatrix}\ddot{\mathbf{u}}^e \\ \ddot{\mathbf{T}}^e\end{Bmatrix} + [\tau_0\mathbf{F}_1\ 0]\begin{Bmatrix}\ddot{\mathbf{u}}_{,x}^e \\ \ddot{\mathbf{T}}_{,x}^e\end{Bmatrix} + [\tau_0\mathbf{F}_2\ 0]\begin{Bmatrix}\ddot{\mathbf{u}}_{,y}^e \\ \ddot{\mathbf{T}}_{,y}^e\end{Bmatrix} \\ &\quad + [\mathbf{F}_1\ 0]\begin{Bmatrix}\dot{\mathbf{u}}_{,x}^e \\ \dot{\mathbf{T}}_{,x}^e\end{Bmatrix} + [\mathbf{F}_2\ 0]\begin{Bmatrix}\dot{\mathbf{u}}_{,y}^e \\ \dot{\mathbf{T}}_{,y}^e\end{Bmatrix} \\ &\quad + [\mathbf{F}_3\ \mathbf{M}_{\theta\theta}]\begin{Bmatrix}\dot{\mathbf{u}}^e \\ \dot{\mathbf{T}}^e\end{Bmatrix} + [0\ -\mathbf{G}_{11}]\begin{Bmatrix}\mathbf{u}_{,xx}^e \\ \mathbf{T}_{,xx}^e\end{Bmatrix} \\ &\quad + [0\ -\mathbf{G}_{22}]\begin{Bmatrix}\mathbf{u}_{,yy}^e \\ \mathbf{T}_{,yy}^e\end{Bmatrix} + [0\ -\mathbf{G}_{33}]\begin{Bmatrix}\mathbf{u}^e \\ \mathbf{T}^e\end{Bmatrix} = \mathbf{Q}^e \end{aligned} \tag{27}$$

We assemble the element matrices into the global matrices in the standard manner to obtain the global governing equation as

$$\mathbf{H}_1\ddot{\mathbf{V}} + \mathbf{H}_2\ddot{\mathbf{V}}_{,x} + \mathbf{H}_3\ddot{\mathbf{V}}_{,y} + \mathbf{H}_4\dot{\mathbf{V}}_{,x} + \mathbf{H}_5\dot{\mathbf{V}}_{,y} + \mathbf{H}_6\dot{\mathbf{V}} + \mathbf{H}_7\mathbf{V}_{,xx} + \mathbf{H}_8\mathbf{V}_{,xy} + \mathbf{H}_9\mathbf{V}_{,yy} + \mathbf{H}_{10}\mathbf{V}_{,x} + \mathbf{H}_{11}\mathbf{V}_{,y} + \mathbf{H}_{12}\mathbf{V} = \mathbf{F} \tag{28}$$

where the matrices $\mathbf{H}_i$ are defined in the appendix and $\mathbf{V}$ is the column vector of assembled nodal displacements and temperatures. In this work, only thermal load is considered. Thus, the vector $\mathbf{F}$ represents the assembled nodal thermal load.

For a wave propagating in the XY plane, we take the Fourier transform of $\mathbf{V}(X, Y, t)$ as

$$\widehat{\mathbf{V}}(k_x, k_y, \omega) = \int_{-\infty}^{\infty}\int_{-\infty}^{\infty}\int_{-\infty}^{\infty}\mathbf{V}(X, Y, t)e^{i(k_xX + k_yY - \omega t)}\,\mathrm{d}X\,\mathrm{d}Y\,\mathrm{d}t \tag{29}$$

Taking the Fourier transform of Eq. (28) and inserting the load vector, the following equation is obtained:

$$[\omega^2\mathbf{H}_1 + i\omega^2k_x\mathbf{H}_2 + i\omega^2k_y\mathbf{H}_3 - \omega k_x\mathbf{H}_4 - \omega k_y\mathbf{H}_5 + i\omega\mathbf{H}_6 + k_x^2\mathbf{H}_7 + k_xk_y\mathbf{H}_8 + k_y^2\mathbf{H}_9 - ik_x\mathbf{H}_{10} - ik_y\mathbf{H}_{11} - \mathbf{H}_{12}]\widehat{\mathbf{V}} = \widehat{\mathbf{F}} \tag{30}$$

where ω is the circular frequency and k_x and k_y are the wave numbers in the X and Y directions, respectively. For a wave propagating in the x-y plane and making an angle θ with the X axis, we have $k_x = k\ \cos\theta$ and $k_y = k\ \sin\theta$. Then, Eq. (30) can be written as

$$(k^2\overline{\mathbf{M}} + k\overline{\mathbf{C}} + \overline{\mathbf{K}})\widehat{\mathbf{V}} = \widehat{\mathbf{F}} \tag{31}$$

where k is the wave number in the propagation direction, and

$$\overline{\mathbf{M}} = -\cos^2\theta\mathbf{H}_7 - \cos\theta\sin\theta\mathbf{H}_8 - \sin^2\theta\mathbf{H}_9 \tag{32}$$

$$\overline{\mathbf{C}} = -i\omega^2\cos\theta\mathbf{H}_2 - i\omega^2\sin\theta\mathbf{H}_3 + \omega\cos\theta\mathbf{H}_4 + \omega\sin\theta\mathbf{H}_5 + i\cos\theta\mathbf{H}_{10} + i\sin\theta\mathbf{H}_{11} \tag{33}$$

$$\overline{\mathbf{K}} = -\omega^2\mathbf{H}_1 - i\omega\mathbf{H}_6 + \mathbf{H}_{12} \tag{34}$$

If the load $\widehat{\mathbf{F}}$ is set equal to zero, then Eq. (31) leads to the eigenvalue problem for finding the wave numbers k of the guided wave modes at a given frequency.

TRANSIENT RESPONSE

In order get the response due to the transient laser thermal load, one can rewrite the equation including the forcing term in the form (see, e.g., Mukdadi and Datta [14] and Liu and Achenbach [15]):

$$[\mathbf{A}]V = \lambda[\mathbf{B}]V + \boldsymbol{P} \tag{35}$$

where

$$\mathbf{A} = \begin{bmatrix} 0 & \mathbf{I} \\ -\overline{\mathbf{K}} & -\overline{\mathbf{C}} \end{bmatrix}, \quad \mathbf{B} = \begin{bmatrix} \mathbf{I} & 0 \\ 0 & \overline{\mathbf{M}} \end{bmatrix}, \quad \lambda = ik$$

and

$$\boldsymbol{V} = \left[\widehat{U}\lambda\widehat{U}\right]^T, \quad \boldsymbol{P} = \left[\widehat{\boldsymbol{F}}\ 0\right]^T$$

The right and left eigenvectors, ϕ_m^R and ϕ_m^L, of the homogeneous form of Eq. (35) satisfy the equations

$$[\mathbf{A} - \lambda_m \mathrm{B}]\phi_m^R = 0, \quad \phi_m^L[\mathbf{A} - \lambda_m \mathrm{B}] = 0 \tag{36}$$

They satisfy the bi-orthogonality conditions

$$\phi_m^L \mathbf{B} \phi_m^R = \mathrm{diag}(\mathbf{B}), \quad \phi_m^L \mathbf{A} \phi_m^R = \mathrm{diag}(\lambda_m \mathbf{B}) \tag{37}$$

Rewriting the right and left eigenvectors as

$$\phi_m^R = \begin{bmatrix} \phi_{mu}^R \\ \phi_{ml}^R \end{bmatrix} = \begin{bmatrix} \phi_{mu}^R \\ \lambda\phi_{mu}^R \end{bmatrix} \quad \text{and} \quad \phi_m^L = [\phi_{mu}^L \quad \phi_{ml}^L] = [\phi_{mu}^L \ \ \lambda\phi_{mu}^L] \tag{38}$$

and substituting Eqs. (38) in Eqs. (37), the bi-orthogonality conditions may be written as

$$\phi_{mu}^L \overline{\mathbf{K}} \phi_{nu}^R + \lambda_m \lambda_n \phi_{mu}^L \overline{\mathbf{M}} \phi_{nu}^R = \delta_{mn} B_n \tag{39a}$$

$$(\lambda_m + \lambda_n)\phi_{mu}^L \overline{\mathbf{K}} \phi_{nu}^R + \lambda_m \lambda_n \phi_{mu}^L \overline{\mathbf{C}} \phi_{nu}^R = \delta_{mn} \lambda_n B_n \tag{39b}$$

Now, the eigenvector $\boldsymbol{V}$ can be expanded in terms of the right eigenvectors ϕ_m^R as

$$\boldsymbol{V} = \sum_{m=1}^{2M} \overline{V}_m \phi_m^R \tag{40}$$

To determine the generalized expansion coefficients $\overline{V}_m$ in the above equation, we substitute expansion (40) in Eq. (35). The resulting equation is

$$[\mathbf{A} - \lambda \mathbf{B}] \sum_{m=1}^{2M} \overline{V}_m \phi_m^R = \boldsymbol{P} \tag{41}$$

Multiplying Eq. (41) by the left eigenvectors ϕ_n^L, one obtains

$$\sum_{n=1}^{2M} \sum_{m=1}^{2M} [\overline{V}_m \phi_n^L \mathbf{A} \phi_m^R - \lambda \overline{V}_m \phi_n^L \mathbf{B} \phi_m^R] = \sum_{n=1}^{2M} \phi_n^L \boldsymbol{P} \tag{42}$$

Now, using the bi-orthogonality conditions (37), the above equation may be simplified to give

$$\sum_{n=1}^{2M}\sum_{m=1}^{2M}[\overline{V}_m\delta_{mn}(\lambda_m-\lambda)\mathbf{B}]=\sum_{n=1}^{2M}\phi_n^L\boldsymbol{P} \tag{43}$$

Solving Eq. (43), one gets

$$\overline{V}_m=\frac{\phi_m^L\boldsymbol{P}}{(\lambda_m-\lambda)B_m}$$

where

$$B_m=\delta_{mn}B_{mn}$$

Equation (40) can then be written as

$$\boldsymbol{V}=\sum_{m=1}^{2M}\frac{\phi_m^L\boldsymbol{P}}{(\lambda_m-\lambda)B_m}\phi_m^R \tag{44}$$

Now, using Eq. (38), the vector $\widehat{U}$ can be expressed as

$$\widehat{U}(\lambda,\omega)=\sum_{m=1}^{2M}\frac{\lambda_m\phi_{mu}^L\widehat{\boldsymbol{F}}}{(\lambda_m-\lambda)B_m}\phi_{mu}^R \tag{45}$$

Taking the inverse Fourier transform of Eq. (45) we obtain

$$\widetilde{U}(\xi;\omega)=\frac{1}{2\pi}\sum_{m=1}^{2M}\int_{-\infty}^{\infty}\frac{\lambda_m\phi_{mu}^L\widehat{\boldsymbol{F}}}{(\lambda_m-\lambda)B_m}\phi_{mu}^Re^{-\lambda\xi}\mathrm{d}\lambda \tag{46}$$

where ξ is the space coordinate in the wave propagation direction. The integral in Eq. (46) is evaluated by using Cauchy's residue theorem. Thus, it is found that

$$\widetilde{U}(\xi;\omega)=-i\sum_{m=1}^{M}\frac{\lambda_m\phi_{mu}^L\widehat{\boldsymbol{F}}}{B_m}\phi_{mu}^Re^{-\lambda_m\xi} \tag{47}$$

To obtain the time-domain response, the inverse Fourier transform of Eq. (47) with respect to ω has to be evaluated numerically. Note that U(ξ, t) is given by

$$U(\xi,t)=\frac{1}{2\pi}\int_{-\infty}^{\infty}\widetilde{U}(\xi;\omega)e^{i\omega t}\mathrm{d}\omega \tag{48}$$

The integral in Eq. (48) has to be evaluated numerically. For dispersive modes, however, difficulties of such integration may occur at the cutoff frequencies ($k=0$)

and at ($\omega = 0$). To circumvent these numerical difficulties, ω is taken to be complex with a small imaginary part. Thus, Eq. (48) is modified to the form

$$U(\xi, t) = \frac{e^{\eta t}}{2\pi} \int_{-\infty}^{\infty} \widetilde{U}(\xi, \omega - i\eta) e^{i\omega t} \mathrm{d}\omega \tag{49}$$

NUMERICAL RESULTS AND DISCUSSION

In this section, we present some representative results obtained by the method described in the previous section. For this purpose, the heat input due to the laser pulse is taken to be given by

$$Q = I_0 f(t) g(x) h(z) \tag{50}$$

where I_0 is the energy absorbed. The temporal profile $f(t)$ is assumed to be of the form

$$f(t) = \frac{t}{t_0^2} \exp\left(\frac{-t}{t_0}\right) \tag{51}$$

Here t_0 is the pulse rise time. The pulse is also assumed to have a Gaussian spatial profile in x, i.e.,

$$g(x) = \frac{1}{2\pi a^2} \exp\left(\frac{-x^2}{a^2}\right) \tag{52}$$

where a is the beam radius. In addition, the depth dependence of Q, which is given by $h(z)$, is taken as

$$h(z) = \gamma e^{-\gamma z} \tag{53}$$

Once Green's function due to $Q = I_0 f(t) h(z) \delta(x)$ is obtained, one can compute the response due to the general form of Q given by Eq. (50) as

$$r(x) = \int_{-\infty}^{\infty} R(\xi) g(\xi - x_0) \mathrm{d}\xi \tag{54}$$

where R is Green's function and x_0 is the coordinate of observation point. The variation of Q along the thickness is modeled by the consistent nodal load representation:

$$h^e = \int_z N_2^e h(z) \mathrm{d}z \tag{55}$$

A schematic representation of the pulse is shown in Figure 3 and the frequency spectrum of $f(t)$ is depicted in Figure 4.

The method outlined above is applicable to any monoclinic thermoelastic plate. Here, numerical results are presented for a silicon nitride (Si_3N_4) plate for

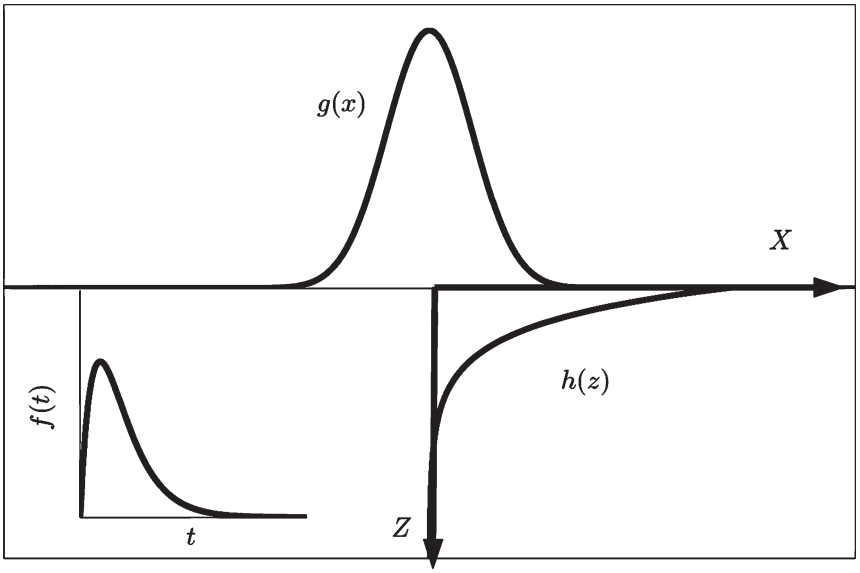

Figure 3 Temporal and spatial profile of the pulse.

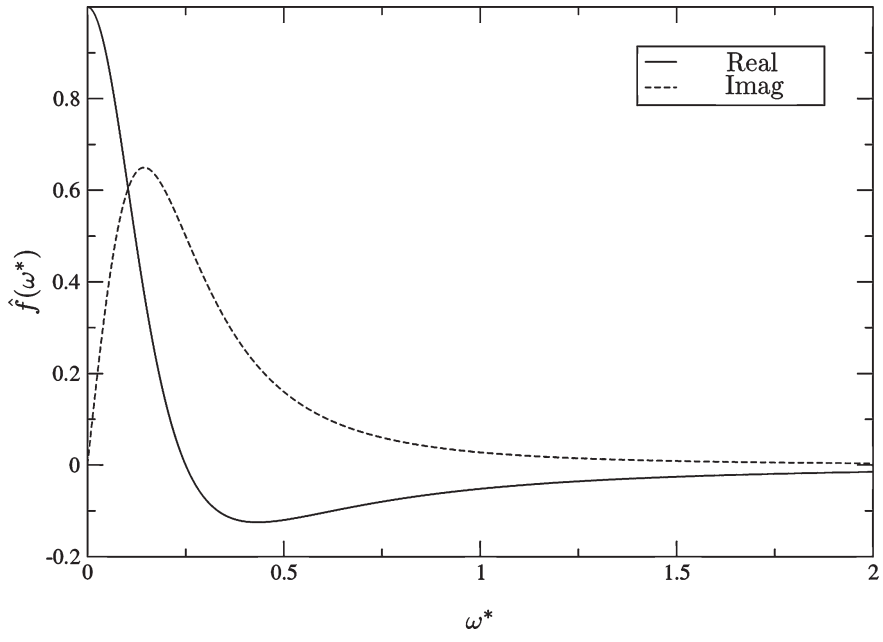

Figure 4 Frequency spectrum of $f(t)$; ω^* is the nondimensional frequency ($\omega^* = \omega H/v_x$).

illustration purposes. The elastic, geometric, and thermal parameters used for the numerical calculations are listed in Table 1.

As stated previously, the homogeneous solution of Eq. (31) yields the dispersion relation of the thermoelastic plate. The dispersion curves for the first few modes have been computed and represented graphically in the form of a 3-D plot in Figure 5. These are obtained by keeping ω real and letting k be complex. The imaginary part of k is a measure of the attenuation of the amplitude with x. Note that 0th-order modes propagate at all frequencies, but the higher order modes have cutoff frequencies below which they are evanescent. Similar to the isothermal case, a complex branch is seen to originate from the minimum point of the S_1 branch. Thermal modes are seen to have high attenuation.

As seen in Figure 4, the frequency spectrum of the pulse is limited to low frequencies ($0 < \omega^* < 1.5$). In this range, primarily the S_0 and A_0 modes are excited. Figure 6 shows transient normal displacement on the x-axis at a source-to-receiver distance of 100 H. The laser is assumed to be focused along the line of the y-axis. The S_0 mode is seen to arrive at the observation point first. This is followed later by the A_0 mode, which is highly dispersive in the frequency range considered. In this case, there is no coupling between SH mode and the S and A modes. So, no SH modes are excited.

Next, the normal displacement was computed at another location, $x = 200\,H$, and is shown in Figure 7. Again, the antisymmetric mode (A_0) dominates, while the symmetric mode is a short-lived event. Moreover, the characteristic dispersion of the antisymmetric mode is clearly seen.

The nondimensional group velocities of the modes propagating along the symmetry direction were computed. These are shown in Figure 8. In the figure, $C_g^* = C_g/v_x$ and $\omega^* = \omega H/v_x$, where $v_x = \sqrt{c_{11}/\rho} = 13.39\,\text{km/s}$. In Figures 6 and 7, the S_0 mode with a group velocity of 0.96 v_x has arrival times of 0.77 and 1.54 microseconds at $x = 100\,H$ and $x = 200\,H$, respectively. Later, the high-frequency components of the A_0 mode arrive with a group velocity of 0.44 v_x. Accordingly, the arrival times of the high-frequency components of the A_0 mode are 1.70 and 3.39 microseconds at $x = 100\,H$ and $x = 200\,H$, respectively. The low-frequency components of the A_0 mode arrive later with much larger amplitude.

In order to see the difference between the response due to the Gaussian spatial distribution $g(x)$ and that due to $\delta(x)$, the normal displacements were calculated at $x = 100\,H$ and $x = 200\,H$ when $g(x) = \delta(x)$ and are shown respectively in Figures 9 and 10 for the two locations. Comparison of the waveforms shown in Figures 6 and 7 with those in Figures 9 and 10 demonstrates the smoothing effect of the Gaussian distribution of the source. It is seen that when the radius of the Gaussian beam goes to zero the high-frequency part of the A_0 mode is excited strongly.

The SAFEM method can be used to investigate wave propagation along any arbitrary direction in the plane of the plate. For this purpose, transient response and group velocities were calculated for two more directions of propagation, namely, $\theta = 45^\circ$ and $\theta = 90^\circ$. Figures 11 and 12 show the transient response for propagation along $\theta = 45^\circ$ at $x = 100\,H$ and $x = 200\,H$, respectively. These figures show clearly the effect of the anisotropy of the plate. The group velocities of the modes propagating in this direction (Figure 13) are different in many ways than for propagation along the symmetry direction. First, the SH modes are now

Table 1 Parameters used in the analysis

Quantity	Units	Numerical value
ρ	Kg/m^3	3.20×10^3
c_{11}	N/m^2	5.74×10^{11}
c_{12}	N/m^2	1.27×10^{11}
c_{22}	N/m^2	4.33×10^{11}
c_{23}	N/m^2	1.95×10^{11}
c_{55}	N/m^2	1.08×10^{11}
T_0	°K	296
β_{xx}	$N/m^2\,°K$	3.22×10^6
β_{yy}	$N/m^2\,°K$	2.71×10^6
C_E	$J/Kg\,°K$	0.67×10^3
K_{xx}	$W/m\,°K$	55.4
K_{yy}	$W/m\,°K$	43.5
t_0	ns	8
τ_0	s	1.44×10^{-13}
a	μm	100
H	mm	0.1
γ	m^{-1}	1×10^5

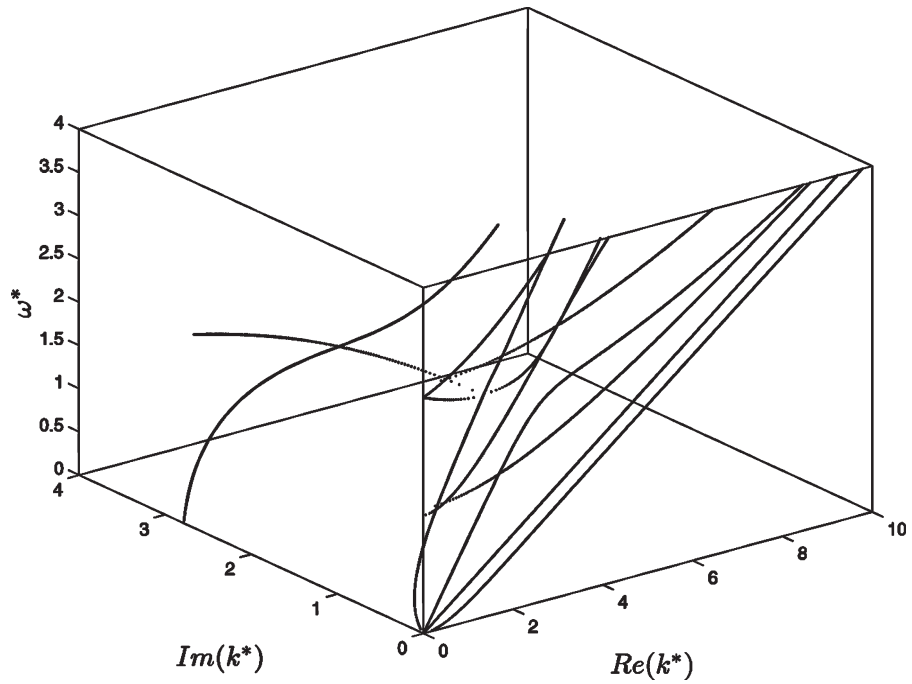

Figure 5 Dispersion curves for guided modes for propagation along the symmetry direction (x-axis) ($\omega^* = \omega H/v_x$ and $k^* = kH$).

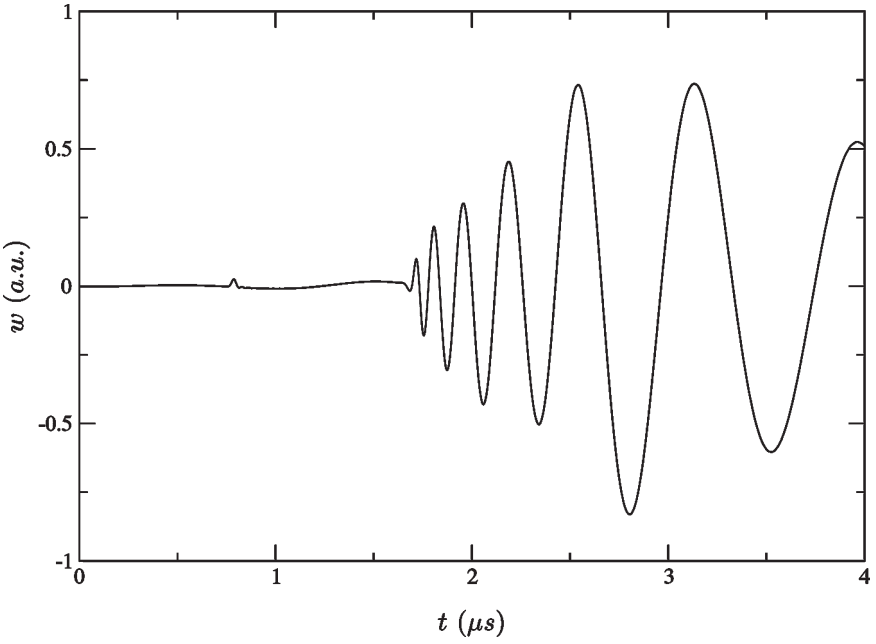

Figure 6 Normal displacement of the plate for propagation along the symmetry direction ($\theta = 0^{\circ}$) at $x = 100\,H$.

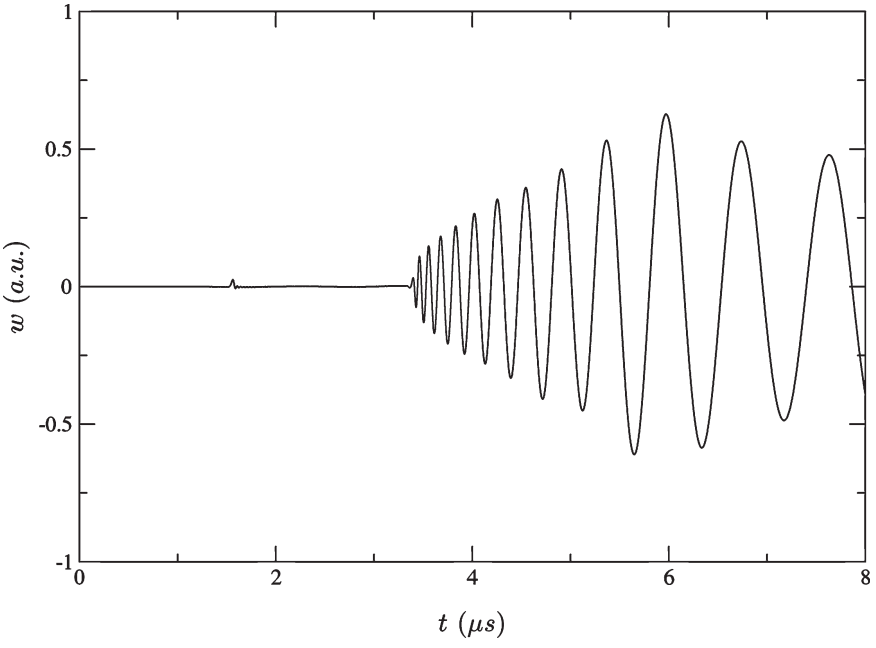

Figure 7 Normal displacement of the plate for propagation along the symmetry direction ($\theta = 0^{\circ}$) at $x = 200\,H$.

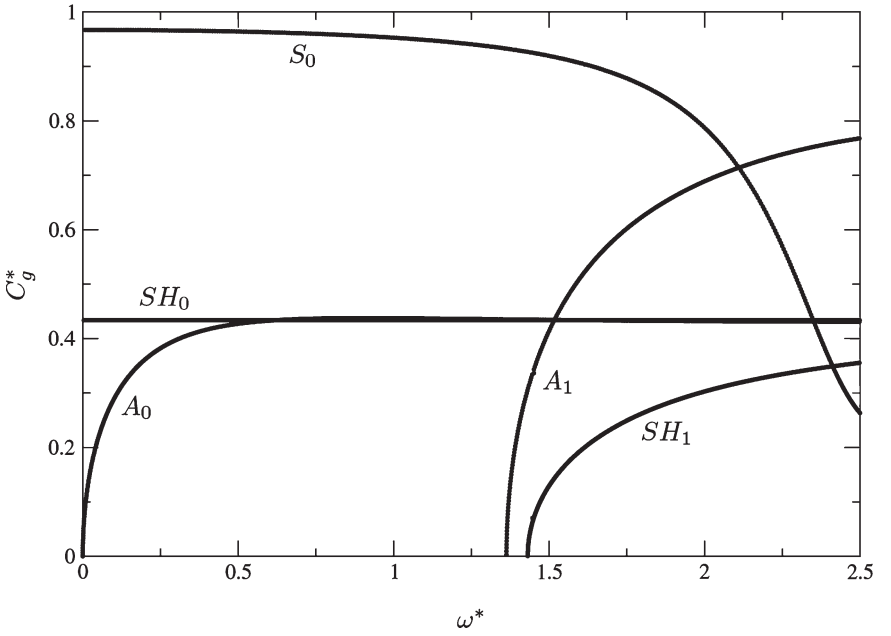

Figure 8 Group velocities of first few modes of propagation along the symmetry direction ($\theta = 0^\circ$).

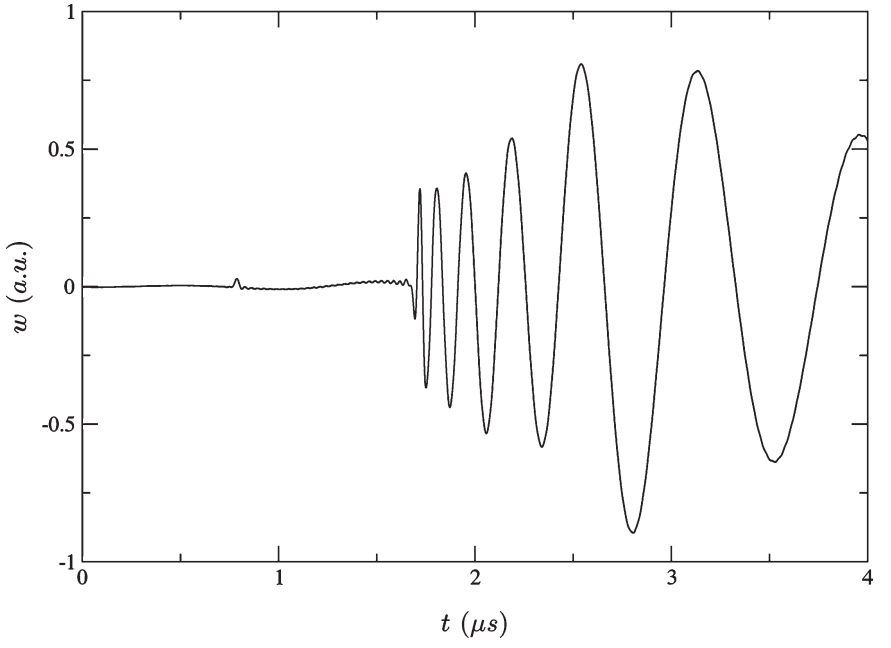

Figure 9 Normal displacement of the plate for propagation along the symmetry direction ($\theta = 0^\circ$) at $x = 100\,H$ when the spatial distribution of the laser pulse is $\delta(x)$.

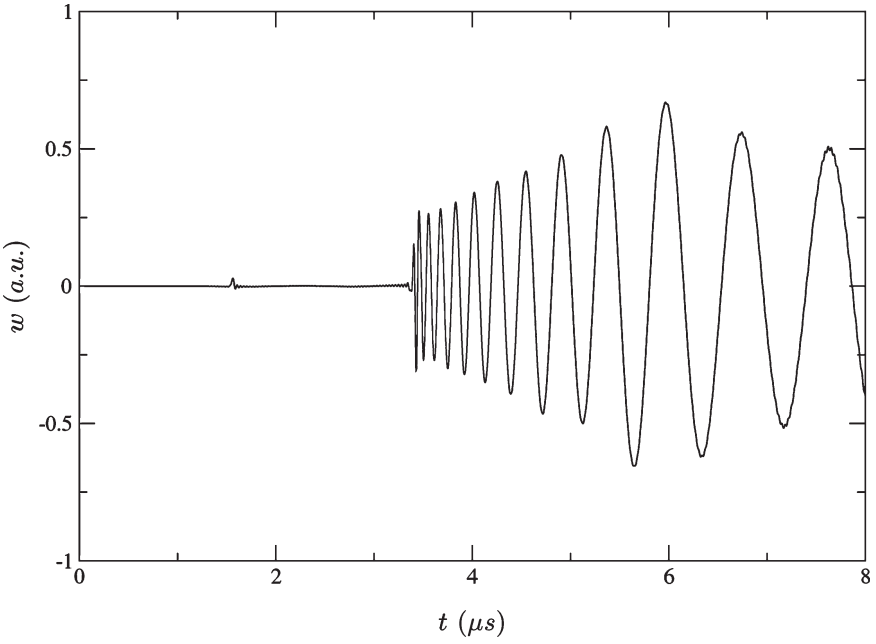

Figure 10 Normal displacement of the plate for propagation along the symmetry direction ($\theta = 0°$) at $x = 200\,H$. The spatial distribution of the pulse is the same as in Figure 9.

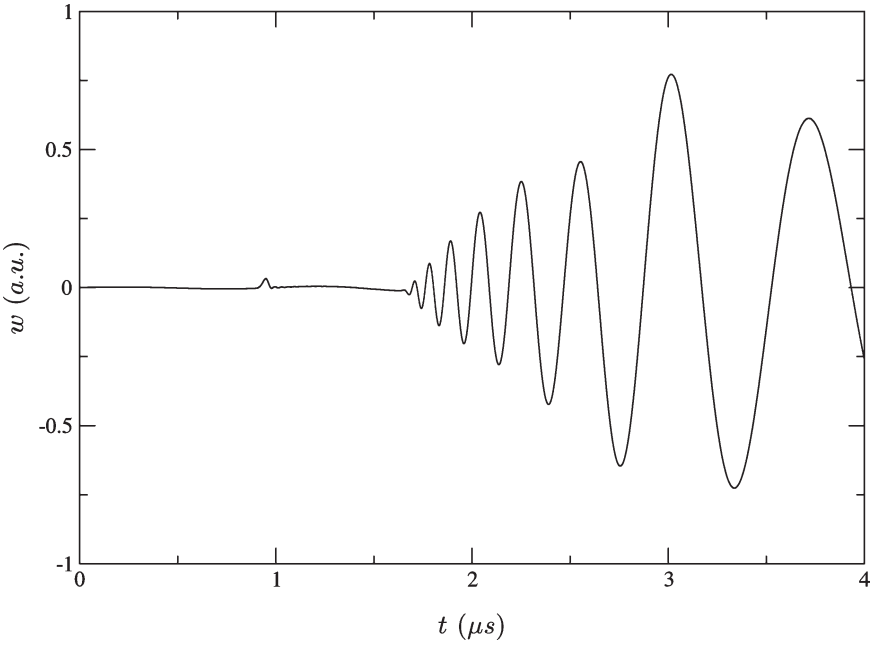

Figure 11 Normal displacement of the plate for propagation along $\theta = 45°$ at $x = 100\,H$.

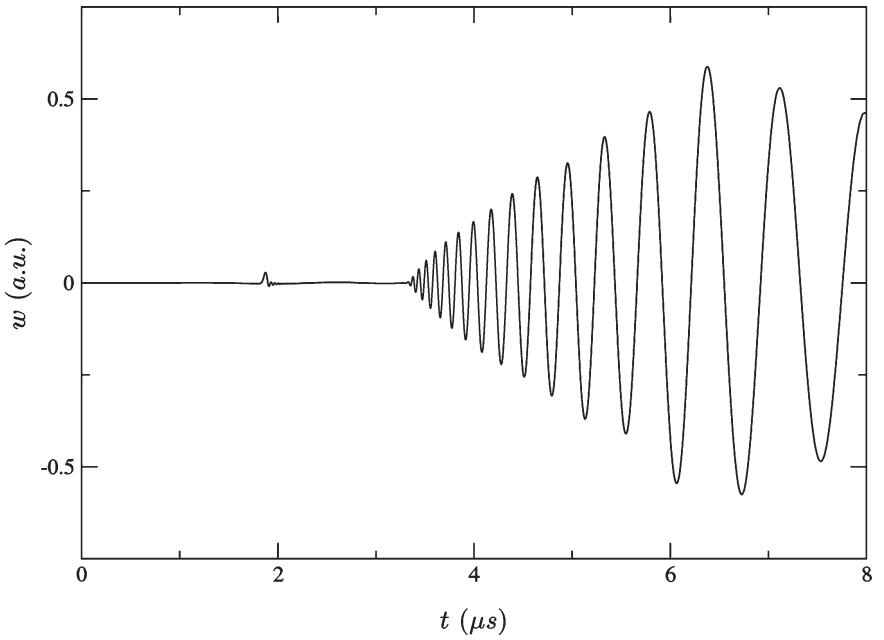

Figure 12 Normal displacement of the plate for propagation along $\theta = 45^\circ$ at $x = 200\,H$.

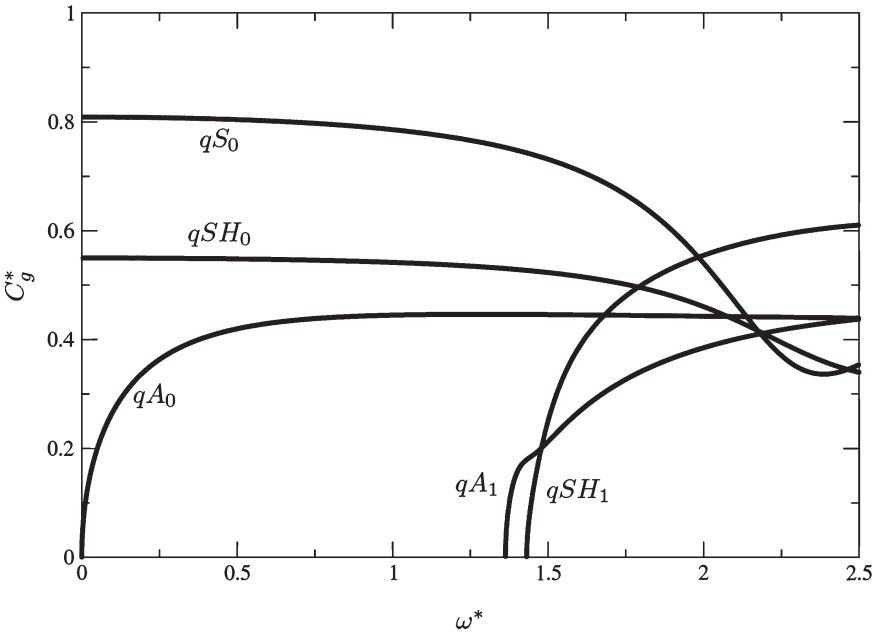

Figure 13 Group velocities of the first few modes of propagation along $\theta = 45^\circ$.

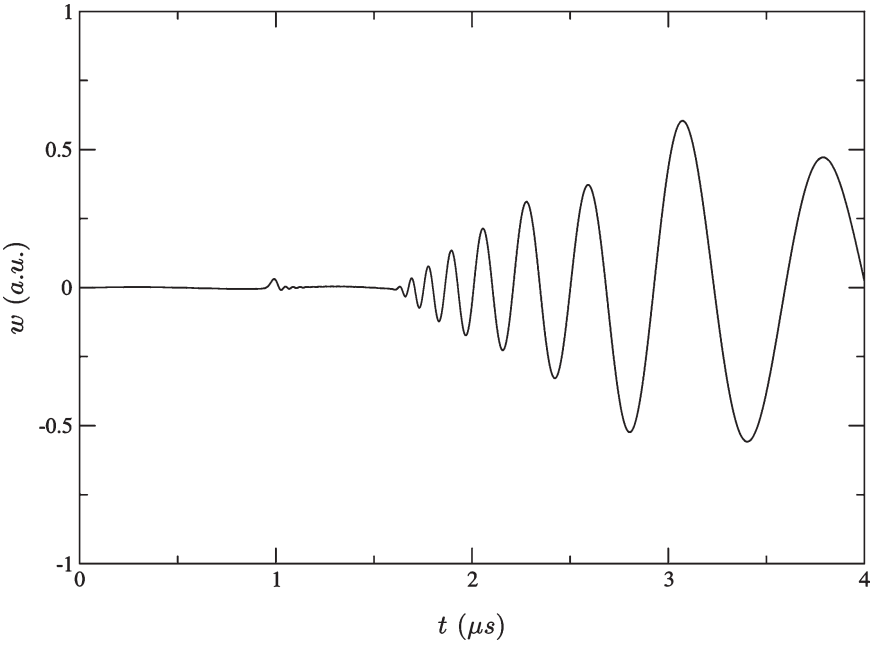

Figure 14 Normal displacement of the plate for propagation along $\theta = 90^\circ$ at $x = 100\,H$.

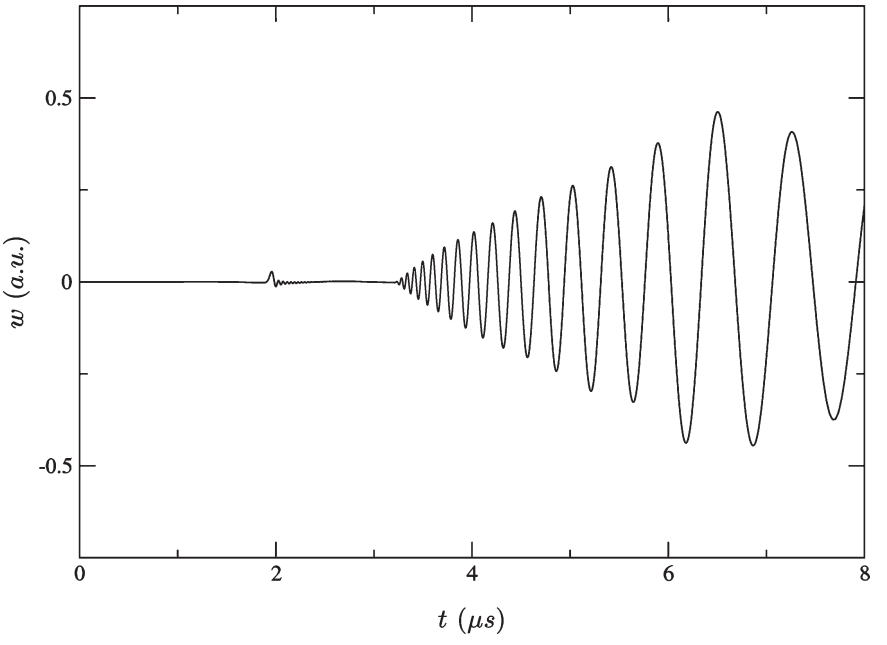

Figure 15 Normal displacement of the plate for propagation along $\theta = 90^\circ$ at $x = 200\,H$.

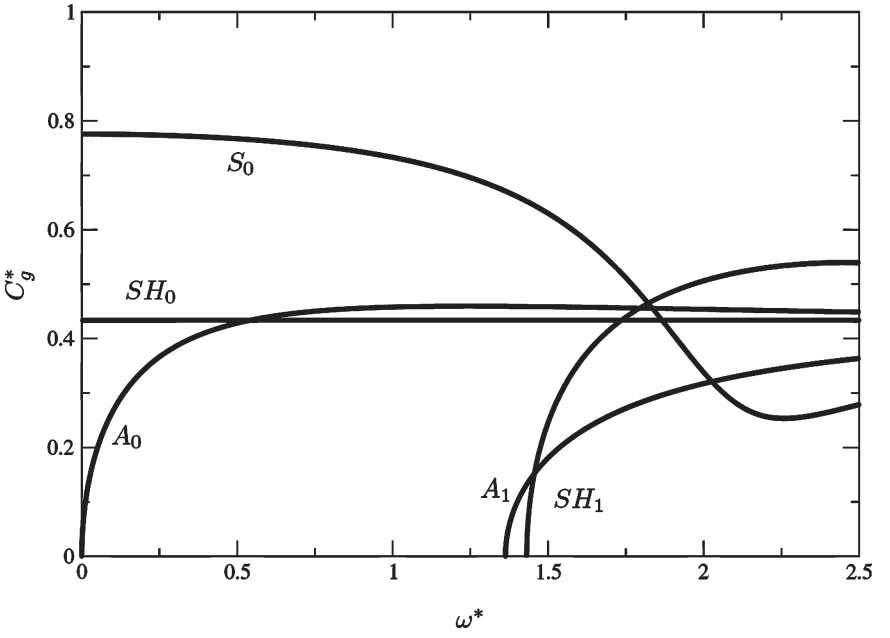

Figure 16 Group velocities of the first few modes of propagation along $\theta = 90^\circ$.

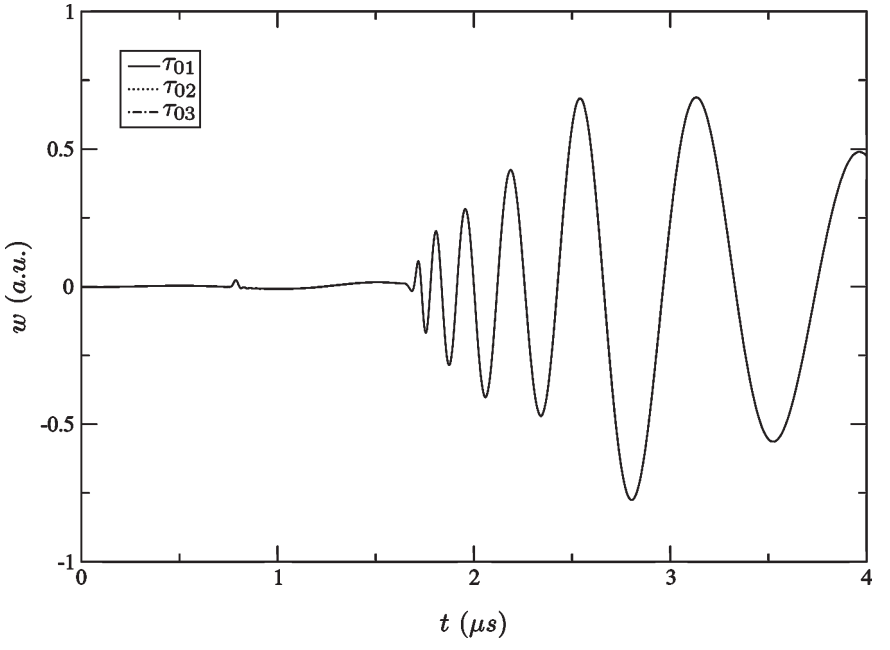

Figure 17 Normal displacement of the plate for three different relaxation times, $\tau_{01} = 0$, $\tau_{02} = 1.44 \times 10^{-13}$ s, and $\tau_{03} = 8 \times 10^{-9}$ s at $x = 100\,H$.

coupled to S and A modes. Note that they are uncoupled for propagation in the symmetry direction. In addition, the group velocities of the S_0 and SH_0 modes are lower. It is interesting to note that the A_0 mode has similar features for propagation in both 0° and 45° directions. Also, the arrival times of the modes are different now. In this case, the group velocities of the S_0 and A_0 modes are, respectively, 0.81 v_x and 0.44 v_x (see Figure 13). These correspond to arrival times of 0.92 and 1.70 microseconds at $x = 100\,H$ and 1.84 and 3.39 microseconds at $x = 200\,H$, respectively. It is seen that the S_0 mode is more dispersive in this direction. This is clearly seen when the observation point is at $x = 200\,H$ (see Figure 12).

Next, transient waveforms and group velocities were computed for $\theta = 90^\circ$. Figures 14 and 15 depict the transient response at the two locations ($x = 100\,H$ and $200\,H$). As noted earlier, the waveforms in this direction are different owing to the anisotropy of the plate. The S_0 mode is slower in this direction with a group velocity of 0.78 v_x. The high-frequency components of the A_0 has a group velocity of 0.45 v_x (see Figure 16). Consequently, the arrival times of both modes at $x = 100\,H$ are, respectively, 0.97 and 1.66 microseconds. They are 1.94 and 3.32 microseconds at $x = 200\,H$. The S_0 mode is more dispersive in this direction. This can be seen in the transient response at larger distance (Figure 15). As in the case of propagation along the symmetry direction, the SH modes are now decoupled from other modes.

Finally, in order to examine the effect of the relaxation time on the transient responses of the plate, normal displacements of the plate were computed for three different relaxation times for propagation along the x-axis. These are shown in Figure 17. It is seen that the transient response is not sensitive to the changes in the relaxation time. Thus, both classical ($\tau_0 = 0$) and hyperbolic ($\tau \neq 0$) heat equations give indistinguishable results for Lamb wave propagation in the plate.

CONCLUSION

Propagation of guided thermoelastic waves in a homogeneous, transversely isotropic, thermally conducting plate was investigated. The dispersion curves and the transient waveforms of Lamb waves in silicon nitride (Si_3N_4) were numerically computed. The results show that thermal modes are much more attenuated than elastic modes. Transient waveforms of Lamb waves indicate that the laser pulse primarily excites the lowest two modes (antisymmetric (A_0) and symmetric (S_0)), where the antisymmetric mode dominates the response. The transient response shows strong dispersion that is characteristic of the A_0 mode. Moreover, it is shown that when the laser beam radius is small the high-frequency components of the A_0 mode are excited strongly. Of particular interest is the observation that the transient response of the plate is insensitive to the changes in the relaxation time.

The results presented here agree with previous experimental (Sontag and Tam [3], Dewhurst et al. [5], Pierce et al. [16]) and theoretical works (e.g., Spicer et al. [6], Cheng and Berthelot [10]). Work is underway to obtain exact solutions to the problem discussed here for some limiting cases and compare the results with those presented here.

REFERENCES

1. C. B. Scruby and L. E. Drain, *Laser Ultrasonics Techniques and Applications*, Adam Hilger, Bristol, 1990.
2. R. White, Generation of Elastic Waves by Transient Surface Heating, *J. Appl. Phys*., vol. 34, pp. 3559–3567, 1963.
3. H. Sontag and A. C. Tam, Optical Monitoring of Photoacoustic Pulse, Propagation in Silicon Wafers, *Appl. Phys. Lett*., vol. 46, pp. 725–727, 1985.
4. D. A. Hutchins, K. Lundgren, and S. B. Palmer, A Laser Study of Transient Lamb Waves in Thin Materials, *J. Acoust. Soc. Am*., vol. 85, pp. 1441–1446, 1989.
5. R. J. Dewhurst, C. Edwards, A. D. W. McKie, and S. B. Palmer, Estimation of the Thickness of Thin Metal Sheet Using Laser Generated Ultrasound, *Appl. Phys. Lett*., vol. 51, pp. 1066–1068, 1987.
6. J. B. Spicer, A. D. W. McKie, and J. W. Wagner, Quantitative Theory for Laser Ultrasonic Waves in a Thin Plate, *Appl. Phys. Lett*., vol. 57, pp. 1882–1884, 1990.
7. R. L. Weaver and Yih-Hsing H. Pao, Axisymmetric Elastic Waves Excited by a Point Source in a Plate, *J. Appl. Mech*., vol. 49, pp. 821–836, 1982.
8. Lei Wu, Jian-chun Cheng, and Shu-yi Zhang, Mechanisms of Laser-Generated Ultrasound in Plates, *J. Phys. D Appl. Phys*., vol. 28, pp. 957–964, 1995.
9. J. C. Cheng, S. Y. Zhang, and L. Wu, Excitations of Thermoelastic Waves in Plates by Pulsed Laser, *Appl. Phys. A Mater*., vol. 61, pp. 311–319, 1995.
10. Jian-Chun Cheng and Yves H. Berthelot, Theory of Laser-Generated Transient Lamb Waves in Orthotropic Plates, *J. Phys. D Appl. Phys*., vol. 29, pp. 1857–1867, 1995.
11. Irene Arias and Jan D. Achenbach, Thermoelastic Generation of Ultrasound by Line-Focused Laser Irradiation, *Int. J. Solids Struct*., vol. 40, pp. 6917–6935, 2003.
12. H. Al-Qahtani and S. Datta, Thermoelastic Waves in an Anisotropic Infinite Plate, *J. Appl. Phys*., vol. 96, pp. 3645–3658, 2004.
13. H. W. Lord and Y. Shulman, A Generalized Dynamical Theory of Thermoelasticity, *J. Mech. Phys. Solids*, vol. 15, pp. 229–301, 1967.
14. Osama M. Mukdadi and Subhendu K. Datta, Transient Ultrasonic Guided Waves in Layered Plates with Rectangular Cross Section, *J. Appl. Phys*., vol. 93, pp. 9360–9370, 2003.
15. G. R. Liu and J. D. Achenbach, Strip Element Method to Analyze Wave Scattering by Cracks in Anisotropic Laminated Plates, *J. Appl. Mech*., vol. 62, pp. 607–613, 1995.
16. S. G. Pierce, B. Culshaw, W. R. Philp, F. Lecuyer, and R. Farlow, Broadband Lamb Wave Measurements in Aluminum and Carbon/Glass Fibre Reinforced Composite Materials Using Non-contacting Laser Generation and Detection, *Ultrasonics*, vol. 35, pp. 105–114, 1997.

APPENDIX: FINITE-ELEMENT MATRICES

$$\mathbf{B}_1 = \begin{bmatrix} N_1 & N_2 & N_3 \\ \cdot & \cdot & \cdot \\ \cdot & \cdot & \cdot \end{bmatrix}, \quad \mathbf{B}_2 = \begin{bmatrix} \cdot & \cdot & \cdot \\ N_1 & N_2 & N_3 \\ \cdot & \cdot & \cdot \end{bmatrix}, \quad \mathbf{B}_3 = \begin{bmatrix} \cdot & \cdot & \cdot \\ \cdot & \cdot & \cdot \\ N_{1,z} & N_{2,z} & N_{3,z} \end{bmatrix}$$

$$\mathbf{D}_1 = \begin{bmatrix} N_1 & \cdot & \cdot & N_2 & \cdot & \cdot & N_3 & \cdot & \cdot \\ \cdot & \cdot & \cdot & \cdot & \cdot & \cdot & \cdot & \cdot & \cdot \\ \cdot & \cdot & \cdot & \cdot & \cdot & \cdot & \cdot & \cdot & \cdot \\ \cdot & \cdot & \cdot & \cdot & \cdot & \cdot & \cdot & \cdot & \cdot \\ \cdot & \cdot & N_1 & \cdot & \cdot & N_2 & \cdot & \cdot & N_3 \\ \cdot & N_1 & \cdot & \cdot & N_2 & \cdot & \cdot & N_3 & \cdot \end{bmatrix},$$

$$\mathbf{D}_2 = \begin{bmatrix} \cdot & \cdot & \cdot & \cdot & \cdot & \cdot & \cdot & \cdot & \cdot \\ \cdot & N_1 & \cdot & \cdot & N_2 & \cdot & \cdot & N_3 & \cdot \\ \cdot & \cdot & \cdot & \cdot & \cdot & \cdot & \cdot & \cdot & \cdot \\ \cdot & \cdot & N_1 & \cdot & \cdot & N_2 & \cdot & \cdot & N_3 \\ \cdot & \cdot & \cdot & \cdot & \cdot & \cdot & \cdot & \cdot & \cdot \\ N_1 & \cdot & \cdot & N_2 & \cdot & \cdot & N_3 & \cdot & \cdot \end{bmatrix}$$

$$\mathbf{D}_3 = \begin{bmatrix} \cdot & \cdot & \cdot & \cdot & \cdot & \cdot & \cdot & \cdot & \cdot \\ \cdot & \cdot & \cdot & \cdot & \cdot & \cdot & \cdot & \cdot & \cdot \\ \cdot & \cdot & N_{1,z} & \cdot & \cdot & N_{2,z} & \cdot & \cdot & N_{3,z} \\ \cdot & N_{1,z} & \cdot & \cdot & N_{2,z} & \cdot & \cdot & N_{3,z} & \cdot \\ N_{1,z} & \cdot & \cdot & N_{2,z} & \cdot & \cdot & N_{3,z} & \cdot & \cdot \\ \cdot & \cdot & \cdot & \cdot & \cdot & \cdot & \cdot & \cdot & \cdot \end{bmatrix}$$

$$\mathbf{k}_{11}^e = \int_z \mathbf{D}_1^T \mathbf{C} \mathbf{D}_1 \mathrm{d}z, \qquad \mathbf{k}_{12}^e = \int_z \mathbf{D}_1^T \mathbf{C} \mathbf{D}_2 \mathrm{d}z,$$

$$\mathbf{k}_{13}^e = \int_z \mathbf{D}_1^T \mathbf{C} \mathbf{D}_3 \mathrm{d}z, \qquad \mathbf{k}_{21}^e = \int_z \mathbf{D}_2^T \mathbf{C} \mathbf{D}_1 \mathrm{d}z,$$

$$\mathbf{k}_{22}^e = \int_z \mathbf{D}_2^T \mathbf{C} \mathbf{D}_2 \mathrm{d}z, \qquad \mathbf{k}_{23}^e = \int_z \mathbf{D}_2^T \mathbf{C} \mathbf{D}_3 \mathrm{d}z,$$

$$\mathbf{k}_{31}^e = \int_z \mathbf{D}_3^T \mathbf{C} \mathbf{D}_1 \mathrm{d}z, \qquad \mathbf{k}_{32}^e = \int_z \mathbf{D}_3^T \mathbf{C} \mathbf{D}_2 \mathrm{d}z,$$

$$\mathbf{k}_{33}^e = \int_z \mathbf{D}_3^T \mathbf{C} \mathbf{D}_3 \mathrm{d}z, \qquad \mathbf{k}_{m01}^e = \int_z \mathbf{D}_1^T \mathbf{C} \beta \mathrm{N}_2^{eT} \mathrm{d}z,$$

$$\mathbf{k}^e_{m02} = \int_z \mathbf{D}_2^T \mathbf{C}\beta \mathbf{N}_2^{eT} \mathrm{d}z, \qquad \mathbf{k}^e_{m03} = \int_z \mathbf{D}_3^T \mathbf{C}\beta \mathbf{N}_2^{eT} \mathrm{d}z$$

$$\mathbf{H}_1 = \begin{bmatrix} -\mathbf{M} & \vdots & 0 \\ \cdots & \cdots & \cdots \\ \tau_0 \mathbf{F}_3 & \vdots & \tau_0 \mathbf{M}_{\theta\theta} \end{bmatrix} \qquad \mathbf{H}_2 = \begin{bmatrix} 0 & \vdots & 0 \\ \cdots & \cdots & \cdots \\ \tau_0 \mathbf{F}_1 & \vdots & 0 \end{bmatrix}$$

$$\mathbf{H}_3 = \begin{bmatrix} 0 & \vdots & 0 \\ \cdots & \cdots & \cdots \\ \tau_0 \mathbf{F}_2 & \vdots & 0 \end{bmatrix} \qquad \mathbf{H}_4 = \begin{bmatrix} 0 & \vdots & 0 \\ \cdots & \cdots & \cdots \\ \mathbf{F}_1 & \vdots & 0 \end{bmatrix}$$

$$\mathbf{H}_5 = \begin{bmatrix} 0 & \vdots & 0 \\ \cdots & \cdots & \cdots \\ \mathbf{F}_2 & \vdots & 0 \end{bmatrix} \qquad \mathbf{H}_6 = \begin{bmatrix} 0 & \vdots & 0 \\ \cdots & \cdots & \cdots \\ \mathbf{F}_3 & \vdots & \mathbf{M}_{\theta\theta} \end{bmatrix}$$

$$\mathbf{H}_7 = \begin{bmatrix} \mathbf{K}_{11} & \vdots & 0 \\ \cdots & \cdots & \cdots \\ 0 & \vdots & -\mathbf{G}_{11} \end{bmatrix} \qquad \mathbf{H}_8 = \begin{bmatrix} \mathbf{K}_{12} + \mathbf{K}_{21} & \vdots & 0 \\ \cdots & \cdots & \cdots \\ 0 & \vdots & 0 \end{bmatrix}$$

$$\mathbf{H}_9 = \begin{bmatrix} \mathbf{K}_{22} & \vdots & 0 \\ \cdots & \cdots & \cdots \\ 0 & \vdots & -\mathbf{G}_{22} \end{bmatrix} \qquad \mathbf{H}_{10} = \begin{bmatrix} \mathbf{K}_{13} - \mathbf{K}_{31} & \vdots & -\mathbf{K}_{m01} \\ \cdots & \cdots & \cdots \\ 0 & \vdots & 0 \end{bmatrix}$$

$$\mathbf{H}_{11} = \begin{bmatrix} \mathbf{K}_{23} - \mathbf{K}_{32} & \vdots & -\mathbf{K}_{m02} \\ \cdots & \cdots & \cdots \\ 0 & \vdots & 0 \end{bmatrix} \qquad \mathbf{H}_{12} = \begin{bmatrix} -\mathbf{K}_{33} & \vdots & -\mathbf{K}_{m03} \\ \cdots & \cdots & \cdots \\ 0 & \vdots & \mathbf{G}_{33} \end{bmatrix}$$